Microstructural Evolution during ARE Process of Al-0.2 mass% Sc Alloy Containing Al3Sc Precipitates in Starting Structures

AUTHOR(S):

Borhani, Ehsan; Jafarian, Hamidreza; Terada, Daisuke; Adachi, Hiroki; Tsuji, Nobuhiro

CITATION:

Borhani, Ehsan ...[et al]. Microstructural Evolution during ARE Process of Al-0.2 mass% Sc Alloy Containing Al3Sc Precipitates in Starting Structures. Materials transactions 2011, 53(1): 72-80

ISSUE DATE:

2011-12

URL:

http://hdl.handle.net/2433/171912

Materials Transactions, Vol. 53, No. 1 (2012) pp. 72 to 80
Special Issue on Advanced Materials Science in Bulk Nanostructured Metals

Microstructural Evolution during ARB Process of Al–0.2 mass% Sc Alloy Containing Al_3Sc Precipitates in Starting Structures

Ehsan Borhani[1,*], Hamidreza Jafarian[1], Daisuke Terada[1], Hiroki Adachi[2] and Nobuhiro Tsuji[1]

[1]*Department of Materials Science and Engineering, Kyoto University, Kyoto 606-8501, Japan*
[2]*Department of Materials Science and Chemistry, University of Hyogo, Himeji 671-2280, Japan*

Effect of pre-existing precipitates on microstructure evolution during severe plastic deformation was studied. An Al–0.2 mass%Sc alloy was aged at 300 and 400°C for having different sizes of Al_3Sc precipitates. The mean precipitate size of Al_3Sc was 3.62 and 50 nm for 300 and 400°C aging, respectively. In the as-aged specimens, Al_3Sc had coherency with the Al matrix. The three kinds of specimens that were solution-treated (ST), aged at 300°C or aged at 400°C, were then heavily deformed by the accumulative roll bonding (ARB) process up to 10 cycles (corresponding to an equivalent strain of 8.0) at room temperature. After 10 cycles of the ARB process, the specimens showed a lamellar boundary structure having the mean lamellar interval of 0.37, 0.24 and 0.27 μm in the ST, 300°C Aged and 400°C Aged specimens, respectively. Additionally, the fraction of high angle grain boundaries (HAGBs) and the average misorientation between boundaries in the Aged-specimens were both higher than those in the ST specimen ARB processed to the same strain. It indicated that grain refinement during the ARB process was accelerated by the pre-existing precipitates. The reasons for the acceleration in microstructural evolution are considered to be the introduction of shear bands, the enhancement of dislocation multiplication rate and the inhibition of grain boundary migration by the precipitates in the pre-aged specimens. [doi:10.2320/matertrans.MD201125]

(Received August 1, 2011; Accepted October 5, 2011; Published December 25, 2011)

Keywords: *accumulative roll bonding (ARB) process, Al_3Sc precipitate, grain refinement*

1. Introduction

Severe plastic deformation (SPD) techniques are now widely applied for the production of ultrafine-grained (UFG) microstructures having mean grain size smaller than 1 μm in bulk metals.[1,2] These techniques have the advantage to produce fully dense materials without introduction of any contamination. Among the various SPD processes, accumulative roll bonding (ARB) is appropriate to manufacture ultrafine grained (UFG) sheet materials, which are the most widely used shape of materials in industry. The ARB allows us to accumulate very large strains into materials without changing the initial dimensions of the materials by repeating the processes of cutting the rolled sheet, stacking them to be the initial thickness and roll-bonding the stacked sheets again, as was explained in elsewhere.[3] In the present investigation, the ARB process was carried out on an Al–0.2 mass%Sc alloy having different starting microstructures, in order to examine the microstructural change of the alloy during the process.

Al–Sc alloys have recently received much interest because of their various advantages. Since fine Al_3Sc precipitates in Al–Sc alloys are thermally stable, grain growth of the matrix grains is greatly inhibited and fine grained structures can be maintained.[4–8] On the other hand, the presence of the second phase particles could potentially have a significant effect on microstructure evolution during the severe plastic deformation processes mentioned above. For example, it is well known that second-phase particles can increase the rate of dislocation generation, and develop local deformation zones containing large local misorientation.[9–11] This can lead to an increased rate in generation of high angle grain boundaries (HAGBs) during plastic deformation.[12–14] However, most of previous researches on the influence of fine particles have been done in low strain deformations, and their effect on the grain refinement through grain subdivision[14,15] by newly generated HAGBs during severe plastic deformation has not been well documented. In this study, pre-aged Al–Sc specimens having two different sizes of precipitates, as well as the solution treated specimen, are prepared and then heavily deformed by the ARB process. The microstructure evolution in the pre-aged specimens is compared with that in the solution treated and ARB processed specimens in order to clarify the effect of pre-existing precipitates.

*Corresponding author, E-mail: ehsan.borhani@ks7.ecs.kyoto-u.ac.jp

2. Experimental Procedure

A binary Al–0.2 mass% Sc alloy was prepared as sheets with thickness of 2 mm, width of 60 mm and length of 200 mm. The chemical composition of the Al–0.2%Sc alloy is given in Table 1.

The sheets were solution treated (ST) at 913 K (630°C) for 86.4 ks and then immediately water-quenched. The average grain size of the matrix in the ST-sheets was 500 μm. Some ST-sheets were aged at 573 K (300°C) or 673 K (400°C) for 10 ks, in order to have two different sizes of Al_3Sc precipitates. The aging conditions were selected according to previous reports.[15,16] Hereafter, those specimens are denoted as Aged-sheets. These ST-sheet and Aged-sheets were used as the starting materials for the ARB process. The starting sheets with the thickness of 2 mm were firstly cold-rolled by 50% reduction in thickness with lubrication. This procedure is considered as the first ARB cycle. A two-high rolling mill with 310 mm diameter rolls was used for rolling at room temperature with lubrication at a rolling speed of 2.0 m min^{-1}. The same conditions were used for roll-bonding

Table 1 Chemical composition of the Al–0.2%Sc alloy studied (mass%).

Si	Fe	Cu	Mn	Mg	Cr	Zn	Ti	Sc
0.016	0.025	0.004	0.001	0.001	0.003	0.001	0.002	0.183

in the subsequent ARB process. In the subsequent ARB process, the 50% cold-rolled sheets with 1 mm thickness were cut into two with the half length in the rolling direction (RD), and then the contact surfaces of the sheets were degreased by acetone and wire-brushed by a stainless steel wire-brush. Two pieces of the sheets were stacked to be 2 mm thick in total and then roll-bonded by 50% reduction in thickness by one pass. The roll-bonded sheets were immediately cooled in water. The same procedures were repeated up to 10 cycles including the first 50% cold-rolling, which corresponded to the total reduction in thickness of 99.9% and the total equivalent strain of 8.0. Hereafter, the ST- and Aged-sheets ARB processed are denoted as ST-ARB, and Aged-ARB specimens, respectively. The starting material and the samples ARB processed by N cycles are expressed as ARB 0c and ARB Nc specimens, respectively.

Sections normal to the transverse direction (TD) of the sheets were used for the microstructural observations. Electron backscattering diffraction (EBSD) analysis was carried out in a scanning electron microscope with a field emission type gun (FE-SEM; Philips XL30) operated at 15 kV. The specimens were mechanically polished and then electro-polished in a solution of 30% HNO_3 and 70% CH_3OH before the measurements. The TEM observations were carried out using Hitachi H-800 operated at 200 kV. Thin foil specimens normal to TD were prepared through mechanical polishing firstly down to approximately 70 µm in the thickness, and then electro-polishing in the same solution as that for the EBSD specimens.

3. Results

3.1 Starting microstructures

Dark field TEM images of three kinds of starting materials before the ARB process obtained from (100) plane diffraction of Al_3Sc are shown in Fig. 1. In the specimen aged at 300°C, there are many fine spherical precipitates with mean particle diameter of 3.62 nm [Fig. 1(a)]. The corresponding diffraction pattern indicates that fine Al_3Sc precipitates have identical orientation as the Al matrix. On the other hand, in the specimen aged at 400°C, there are coarse and cauliflower shaped precipitates with a mean size of around 50 nm in diameter [Fig. 1(b)]. The corresponding diffraction pattern shows that the coarse Al_3Sc precipitates also have an identical orientation relationship with the matrix and probably keep coherency. Furthermore, no precipitate is

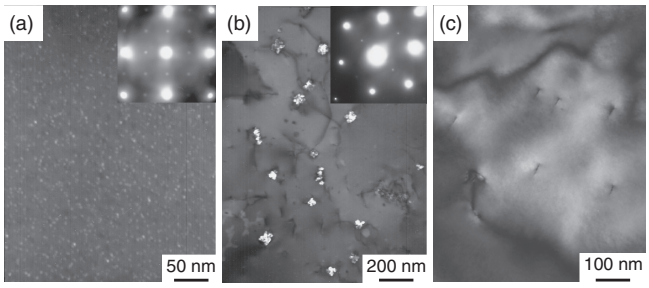

Fig. 1 Dark field TEM micrographs of (a) 300°C Aged specimen, (b) 400°C Aged specimen and (c) ST specimen obtained from (100) diffraction of Al_3Sc.

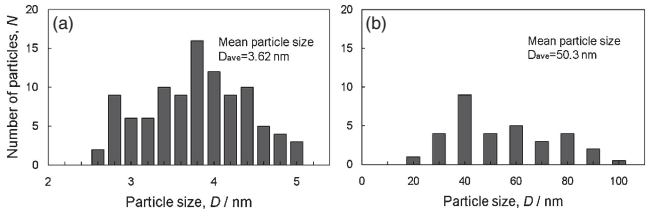

Fig. 2 Size distribution of the Al_3Sc particles in (a) 300°C aged specimen and (b) 400°C aged specimen.

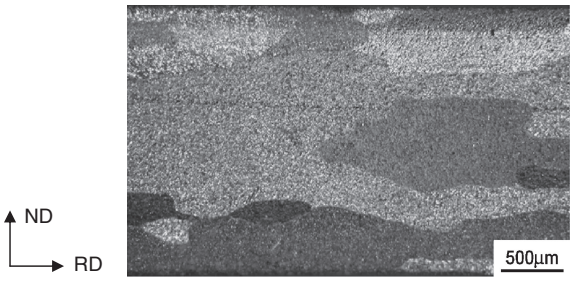

Fig. 3 Optical micrograph of the ST-specimen containing coarse grains.

observed in the solution treated specimen [Fig. 1(c)]. The size distribution of the precipitates in the aged specimens is also plotted in Fig. 2. It is seen in Fig. 2 that the distribution of precipitates in the 300°C Aged specimen is rather homogeneous containing lower range particle sizes than that of the 400°C Aged specimens.

3.2 Microstructure evolution in matrix during ARB process

Figure 3 shows an optical micrograph of the ST specimen before the ARB process, containing coarse original grains of about 500 µm in size. The aged specimen also had similar grain size of the matrix. Grain boundary maps obtained from EBSD analysis of the ST-, 300°C Aged- and 400°C Aged-specimens after various cycles (strains) of the ARB are shown in Fig. 4. The boundaries are classified into low-angle grain boundaries (LAGBs) with misorientation (θ) of $2° \leq \theta < 15°$ drawn in red, and high-angle grain boundaries (HAGBs) with $\theta \geq 15°$ drawn in green. Boundaries having misorientation smaller than 2° were cut off, in order to remove inaccuracy in EBSD measurement and analysis.

At the initial stages of the ARB process (1 cycle and 3 cycles in Fig. 4 corresponding to equivalent strain $\varepsilon = 0.8$ and 2.4, respectively) the microstructures of the matrix are non-uniform and consist of two kinds of grain sizes, i.e., fine grains and very coarse and elongated grains which correspond to the initial grains. The specimens ARB processed below 3 cycles ($\varepsilon = 2.4$) show inhomogeneous microstructures which consist of fine grains surrounded by HAGBs and relatively large grains including LAGBs. It seems that the number of the fine grains surrounded by HAGBs and the amount of LAGBs are both larger in the 300°C Aged-ARB specimen than those in the other specimens. It is found that the 300°C Aged-ARB specimen shows large number of LAGBs aligned to specific orientations to RD, i.e., several LAGBs have a slope of approximately 45° against RD, which correspond to local shear bands shown later.

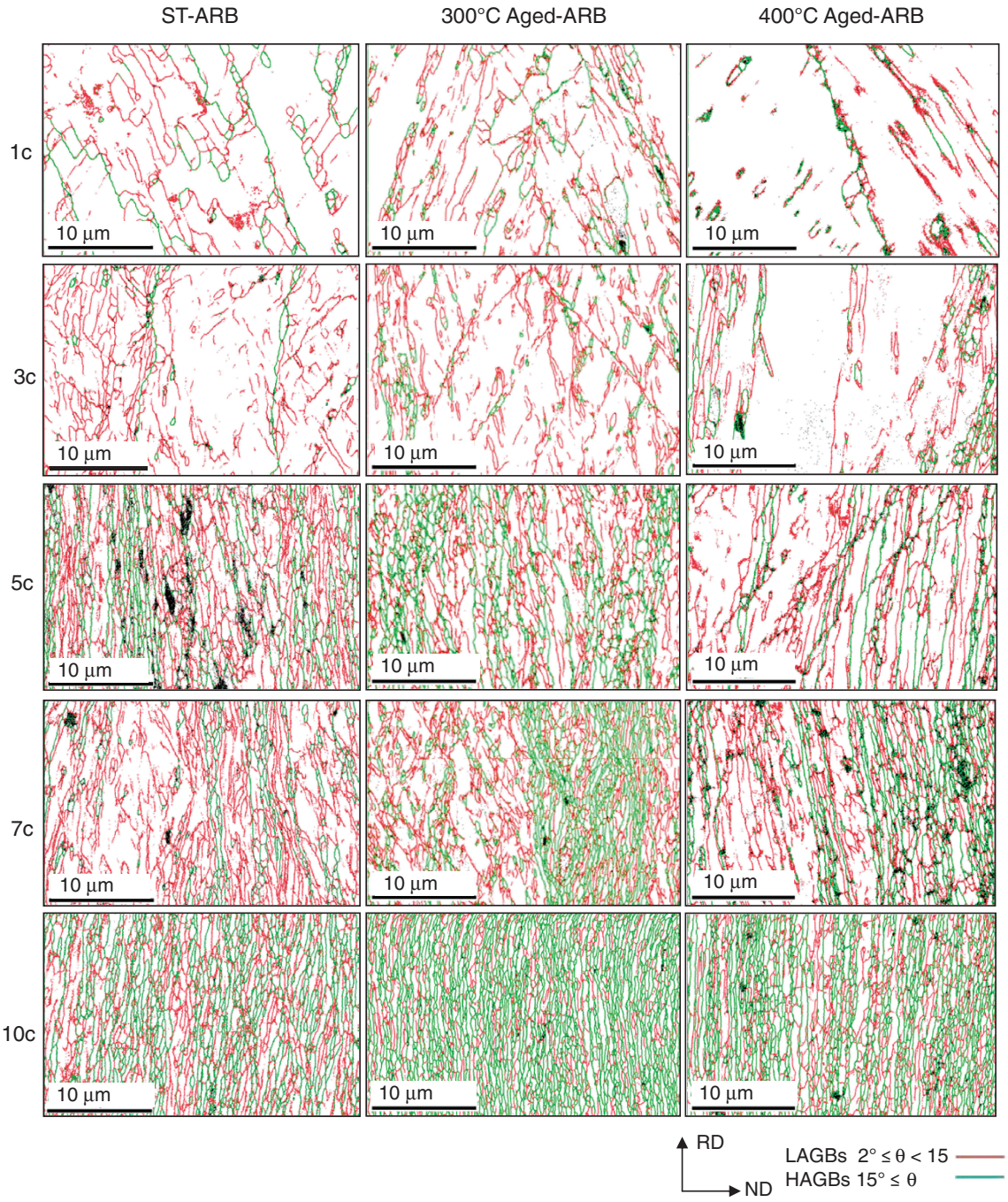

Fig. 4 Grain boundary maps obtained from EBSD measurement for the ST- and Aged-specimens ARB processed by various cycles up to 10 cycles at room temperature.

After the ARB process up to medium cycles (5 and 7 cycles corresponding to $\varepsilon = 4.0$ and 5.6, respectively), the microstructures are still inhomogeneous. Some regions include relatively high density of LAGBs and the other regions show elongated UFG structures with high density of HAGBs. It is found that the fraction of HAGBs in the 300°C Aged-ARB specimen is the largest among the specimens.

In the specimens ARB processed by 10 cycles ($\varepsilon = 8.0$), microstructures are homogeneous compared with the specimens ARB processed below 7 cycles. The specimens show lamellar boundary structures elongated along RD. In the two kinds of aged specimens having precipitates, the distribution of HAGBs is relatively homogeneous, and the most of grains are surrounded by HAGBs. It is found that the HAGB spacing in the 300°C Aged-ARB specimen is smaller than that of the 400°C Aged-ARB specimen. On the other hand, the coarse regions without HAGBs are retained in the ST-ARB specimen processed by 10 cycles. The HAGBs spacing in the ST-ARB specimen is larger than those in the Aged-ARB specimens.

From the results of the EBSD measurements, it is considered that grain refinement by severe plastic deformation is accelerated by pre-existing precipitates. This acceleration is presumably attributed to inhibition of dislocation motion by the precipitates. Additionally, the smaller precipitate seems to be more effective for grain-refinement.

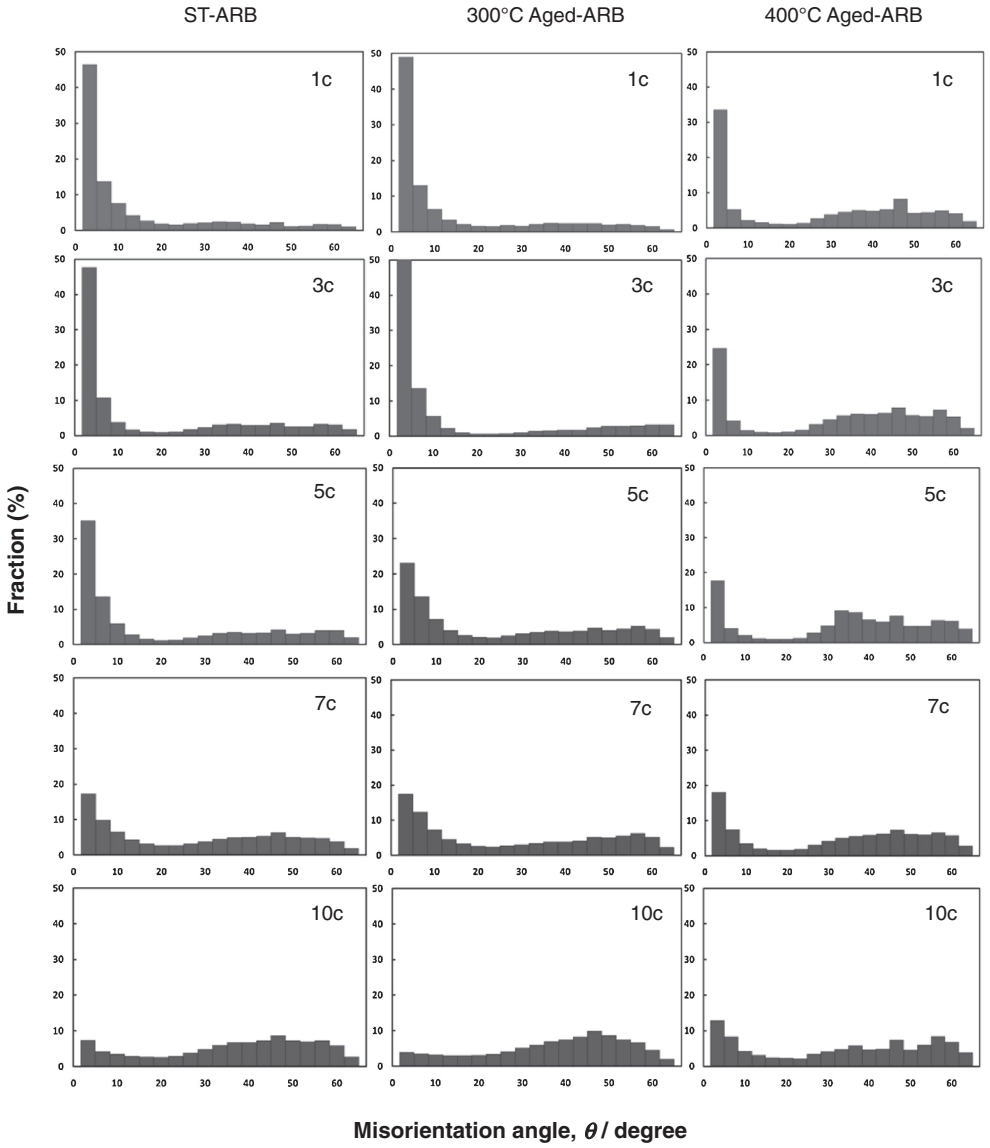

Fig. 5 Misorientation distribution in the ST- and Aged-specimens ARB processed by various cycles.

3.3 Quantification of microstructure evolution

The misorientation distribution obtained from EBSD measurements of the ARB processed specimens are given in Fig. 5 as fraction-misorientation histograms. The misorientation was calculated between neighboring measured points in the EBSD mapping data by software (OIM analysis version 5.6).

After 1 and 3 cycles, the shape of histograms is similar, and the fraction of boundaries with misorientation smaller than 5° is very high. It reflects that dislocations or LAGBs were introduced during ARB process. In the specimens ARB-processed above 5 cycles, the fraction of small misorientation decreased gradually with increasing the number of ARB cycles while the fraction of HAGBs increased. After 10 cycles, the fraction of LAGBs in the ST-ARB and 300°C Aged-ARB specimens decreased to less than 10%. In these specimens, the fraction of misorientation ranging from 45 to 50° is the highest. The distribution becomes close to a random distribution of misorientation.[15,16] On the other hand, the fraction of the LAGBs in the 400°C Aged-ARB specimen kept more than 10% after 10 cycles ARB.

The grain size, d_t, is given in Fig. 6(a). The d_t is evaluated as the mean spacing of HAGBs along ND by linear intercept method in the EBSD boundary maps. From the figure, it is found that the d_t decreases with increasing the number of ARB cycles. After 1 cycle of ARB processing, the d_t of the 300°C Aged-ARB, 400°C Aged-ARB and ST-ARB specimens are 0.9, 2.3 and 2.1 µm, respectively, though the initial grain size was several hundred micrometers. The d_t of the specimens decreases down to approximately 0.4 µm with increasing ARB cycle up to 5 cycles. Afterward, the d_t decreases with increasing the number of ARB cycles.

The d_t of the 300°C Aged-ARB specimen is much smaller than that of the other specimens below 5 cycles. It indicates that the fine precipitates in the 300°C Aged-ARB specimen enhances the rate of grain-refinement during the ARB process. After 10 cycles of ARB processing, the d_t reduces down to 0.24, 0.27 and 0.37 µm for the 300°C Aged-ARB, 400°C Aged-ARB and ST-ARB specimens, respectively.

The above results mean that the fine Al_3Sc precipitates in the 300°C Aged-ARB specimen dominantly affect the grain

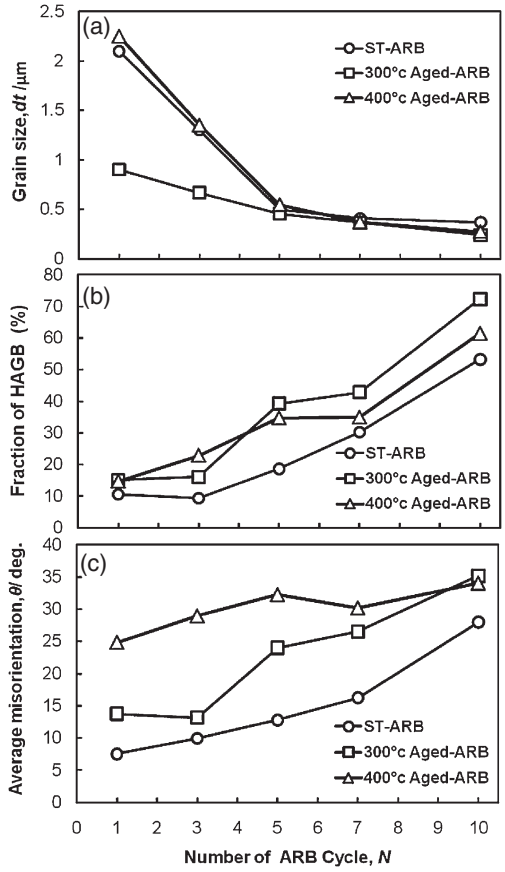

Fig. 6 Change in average grain size (a), fraction of high angle boundary (b) and average misorientation (c) as a function of the number of ARB cycles.

refinement up to 5 cycles, but the influence of the precipitates at 10 cycles is not as obvious as in the specimens ARB processed to 5 cycles. This indicates that the fine pre-existing precipitates have a significant effect on microstructure evolution at relatively low applied strains.

The fraction of HAGBs, f_{HAGBs}, is plotted as a function of the number of ARB cycles in Fig. 6(b). The f_{HAGBs} increases monotonically with increasing the number of ARB cycles. It is found that the f_{HAGBs} of the ST-ARB specimen is always lower than those of the 300°C Aged-ARB and 400°C Aged-ARB specimens at the same ARB cycle. Additionally, the f_{HAGBs} of the 300°C Aged-ARB specimen is larger than that of the 400°C Aged-ARB specimen. Finally, after 10 cycles, the f_{HAGBs} of the 300°C Aged-ARB, 400°C Aged-ARB and ST-ARB specimens is 72.4, 61.6 and 53.28%, respectively. These results show that the rate of HAGBs formation was also affected by the pre-existing precipitate, and that the finer precipitates were more effective for forming HAGBs during the ARB process.

Figure 6(c) shows the average misorientation angle, θ, as a function of ARB cycles. It can be seen that the average misorientation angle increases with increasing the number of ARB cycles in all specimens. It is found that the average misorientation angles in the two kinds of the Aged-ARB specimens are higher than that of the ST-ARB specimen. In the 300°C Aged-ARB and ST-ARB specimens, the average misorientation angle increased monotonically with increasing the number of ARB cycles up to 10 cycles. In case of the

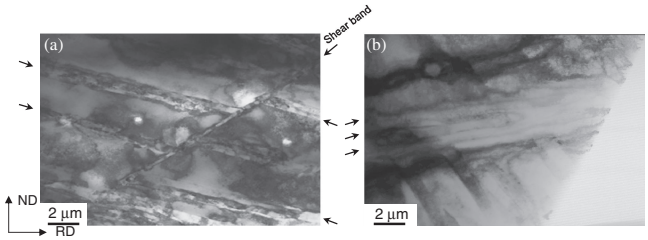

Fig. 7 TEM micrographs of (a) 300°C Aged-ARB 1c specimens and (b) 400°C Aged-ARB 1c specimen.

400°C Aged-ARB specimens, the average misorientation increases up to 5 cycles, then keeps a constant value. Furthermore, the 400°C Aged-ARB specimen has higher misorientation angle than that of the 300°C Aged-ARB specimen, although they have almost the same value of mean misorientation at the ARB 10 cycles.

3.4 TEM observation of ARB processed specimens

Figure 7 shows the TEM micrographs of the 300°C Aged-ARB and 400°C Aged-ARB specimens processed by 1 cycle. The typical pictures were chosen from several TEM micrographs observed for each kind of specimen. Some shear bands indicated by arrows are observed, though shear bands have not been observed in the ST-ARB specimen[17] and pure aluminum in previous studies.[18–20] These results indicate that shear bands introduced during the ARB process are caused by the presence of pre-existing precipitates. The shear bands correspond to the aligned LAGBs observed in EBSD maps (Fig. 4) which had a slope of approximately 45° against RD. Fine lamellar boundary structures are found within the shear bands in TEM [Fig. 7(b)]. From the figures, width of the shear bands in the 300°C Aged-ARB specimen is smaller and the number of the shear bands in the 300°C Aged-ARB specimen is somehow larger than those in the 400°C Aged-ARB specimen. This fact was also confirmed in large scale EBSD maps with size area of 500 μm × 100 μm. It is considered that the finer precipitates enhance to introduce shear bands much more effectively. Introduction of shear bands during SPD processes have been also reported elsewhere.[10,11,21–23]

Typical TEM microstructures of the Aged-ARB specimens after 1 cycle are shown in Figs. 8(a) and 8(b). The microstructures indicate that the Al_3Sc precipitates are distributed randomly in the matrix. It is also observed that a high-density of dislocations interact with Al_3Sc precipitates especially in the 400°C Aged-ARB specimen. It is expected that the accumulation of dislocations was accelerated because the dislocation motion is inhibited by the precipitates during the ARB process.

Figure 9 shows TEM micrographs of the ST-ARB, 300°C Aged-ARB and 400°C Aged-ARB specimens processed by 9 cycles. The TEM micrographs were observed from TD. From the figures [Figs. 9(a)–9(c)], the specimens ARB processed by 9 cycles show lamellar boundary structure elongated along RD which is a typical ultra-fine microstructure formed by the ARB process.[24,25] The mean boundary spacing parallel to ND is approximately 500 nm. The shear bands were not observed after 9 cycles.

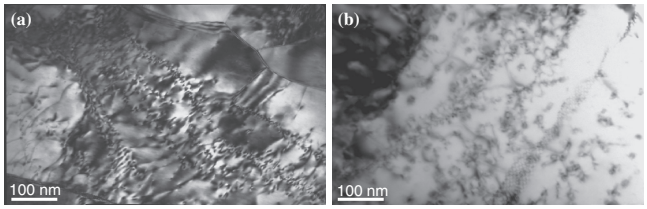

Fig. 8 TEM micrographs of the Al–0.2Sc alloy of (a) 300°C Aged-ARB 1c and (b) 400°C Aged-ARB 1c specimens.

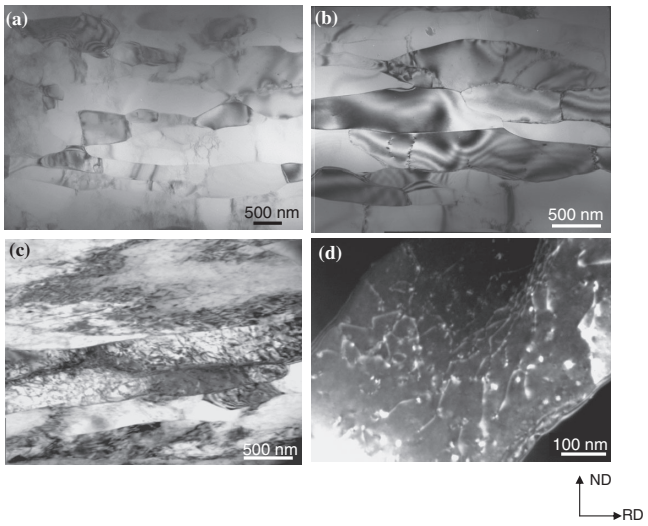

Fig. 9 TEM micrographs of (a) ST-ARB 9c and (b) 300°C Aged-ARB 9c, (c) 400°C Aged-ARB 9c specimens and (d) 400°C Aged-ARB 10c specimens.

In case of the ST-ARB and 300°C Aged-ARB 10c specimens [Figs. 9(a) and 9(b)], it seems that dislocation density is fairly low within the lamellar grains. On the other hand, large number of dislocations seems to exist within the elongated grains in the 400°C Aged-ARB specimen [Fig. 9(c)]. Figure 9(d) shows a TEM micrograph obtained by dark field method for the 400°C Aged-ARB specimen processed by 10 cycles. Dislocations are clearly observed within the lamellar grains.

3.5 Change in precipitates in aged-specimens during ARB process

In this section the change in Al_3Sc precipitate in the aged specimens during the ARB process is focused and discussed. A TEM micrograph of the 300°C Aged-ARB specimen after 1 cycle ARB is shown in Fig. 10. Figure 10(b) is a selected area diffraction (SAD) pattern obtained from Fig. 10(a). Figure 10(c) is a key diagram corresponding to the SAD pattern. In this TEM micrograph, although it is difficult to observe very fine precipitates, the diffraction pattern includes the diffraction spots corresponding to Al_3Sc precipitate, which are indicated by white arrows in Fig. 10(b). From the SAD pattern, it is found that, the crystal plane (100) and (110) of the Al_3Sc precipitate are parallel to the crystal plane (200) and (220) of the Al matrix, respectively. The results indicate that the precipitates keep an orientation relationship with the matrix after 1 cycle of ARB process. Thus, it is expected that the precipitation might keep coherency to the matrix after 1 cycle ARB process.

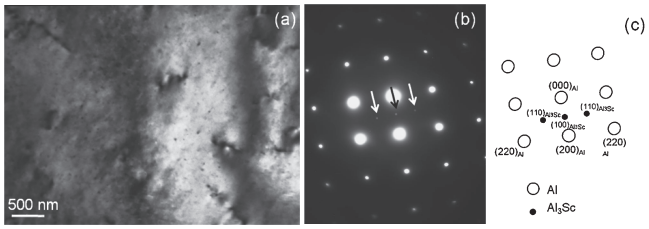

Fig. 10 TEM micrographs of the 300°C Aged-ARB specimen after 1 cycle ARB process. (a) TEM microstructure, (b) SAD pattern and (c) a key diagram.

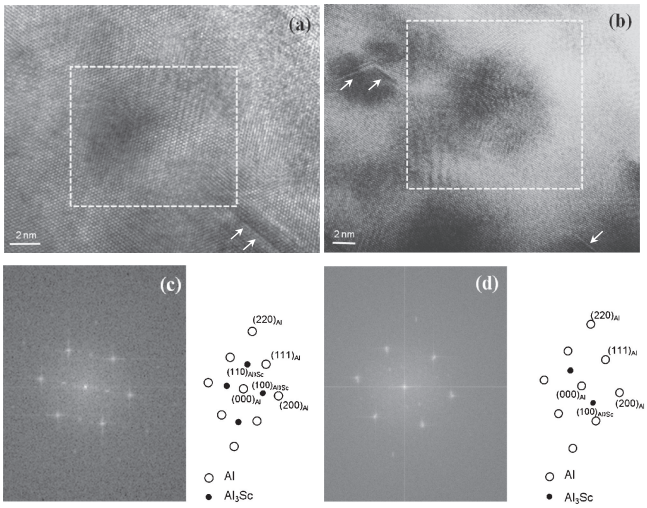

Fig. 11 TEM images of Al_3Sc precipitates in the 300°C Aged-ARB specimen after 9 cycles of ARB. (a) precipitates having the identical orientation relationship with matrix and (b) precipitates with different orientation relationship with matrix. (c) and (d) are corresponding diffraction patterns obtained by FFT analysis for the areas surrounded by white-broken lines in (a) and (b), respectively.

High resolution TEM (HRTEM) micrographs of the 300°C Aged-ARB specimen after 9 cycles are shown in Figs. 11(a) and 11(b). Several straight lines indicated by arrows due to stacking faults are observed in these figures. Tetragonal regions in the images surrounded by white broken lines were analyzed by fast Fourier transformation (FFT). The results of the FFT analysis corresponding to diffraction patterns are given in Figs. 11(c) and 11(d) with related key diagrams. From Fig. 11(c), it is found that the precipitate in Fig. 11(a) keeps the particular orientation relationship with the matrix, which was found in the aged specimens before ARB process. On the other hand, the orientation relationship between the precipitates and the matrix in Fig. 11(b) is different from that confirmed in the starting microstructure of the Aged specimens. It can be concluded, therefore, that the orientation relationship between some precipitates and matrix is changed during ARB process.

TEM microstructures of the 400°C Aged-ARB specimen processed by 1 cycle are shown in Fig. 12. Figure 12(a) shows a bright field image, (b) shows a dark field image corresponding to a diffraction spot of Al_3Sc precipitate, and (c) is the corresponding diffraction pattern with key diagrams. From these figures, it is obvious that precipitates keep the identical orientation to the Al matrix. An HRTEM

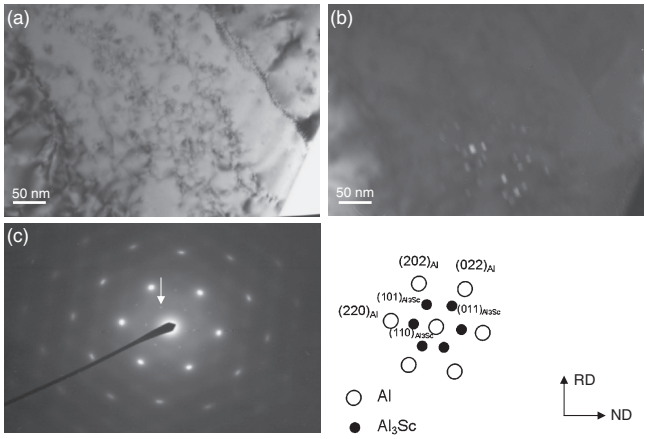

Fig. 12 TEM micrographs of the 400°C Aged-ARB specimen deformed by ARB by 1 cycle: (a) Bright field image, (b) dark field image and (c) SAD patterns.

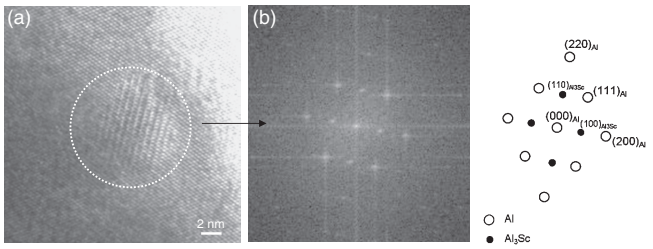

Fig. 13 High-resolution TEM images of Al_3Sc precipitates formed at 400°C for 10 Ks and then deformed by ARB up to 9 cycles. (a) A coherent precipitate (surrounded by dotted circle), and (b) corresponding Furrier analyzed pattern for (a).

micrograph of the 400°C Aged-ARB specimen after 9 cycles is shown in Fig. 13 with the FFT image and the key diagram.

TEM micrographs of the 400°C Aged-ARB specimen processed by 10 cycles are shown in Fig. 14. The diffraction pattern obtained from the region surrounded by a circle of broken line in Fig. 14(a) is shown in (b). In Fig. 14(b), two kinds of diffraction spots indicated by arrows 1 and 2 are observed. Both of the spots correspond to Al_3Sc precipitates. Figures 14(c) and 14(d) show the dark field images corresponding to the arrow 1 and arrow 2, respectively. It appears that the diffraction spot indicated by the arrow 1 keeps a specific orientation relationship between the precipitates and matrix. On the other hand, the diffraction spot indicated by the arrow 2 is deviated from the position for a diffraction spot shown by arrow 1. It is found that the brightness of precipitates are different between Figs. 14(c) and 14(d). The results indicate that orientation relationship between Al_3Sc precipitates and matrix in the 400°C Aged specimen is changed even within the identical matrix grain, probably due to plastic deformation during 9-cycle ARB.

Additionally, it is noteworthy that the precipitates showing spherical morphology have an average diameter of approximately 10 nm after 9 cycles of ARB process, although the cauliflower shaped precipitates had mean particle size of 50 nm prior to the ARB process. It is expected that the coarse Al_3Sc precipitates are dissolved and re-precipitated, or fragmented into small ones during the ARB process.

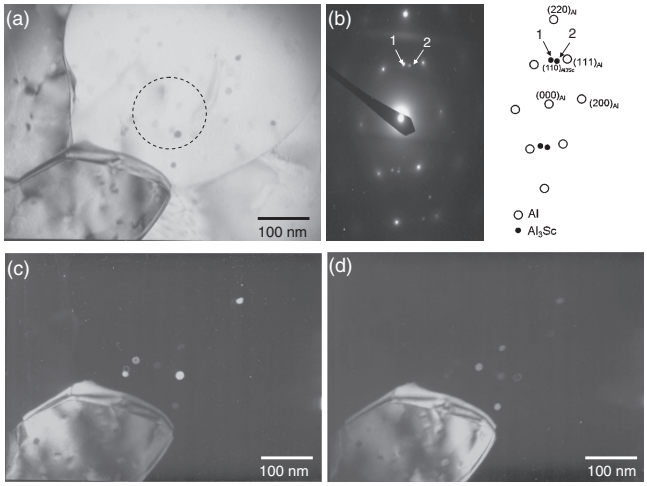

Fig. 14 TEM micrographs of the (a) bright field, (b) diffraction pattern obtained from the surrounded region in (a), (c) and (d) dark field images corresponding to the arrow 1 and arrow 2, respectively, showing different orientation of Al_3Sc particles with respect to the matrix in the 400°C Aged-ARB 10c specimens.

4. Discussion: Effect of Pre-Existing Precipitates on Microstructural Evolution

From the microstructural observations, it was found that the grain refinement during the ARB process was accelerated by the pre-existing precipitates. For example, the fraction of HAGBs and the average misorientation in the Aged-specimens including the pre-existing precipitates were higher than those of the ST-specimen at the same ARB cycle (Fig. 6). At low ARB cycles, the grain size of the 300°C Aged-ARB specimen was much smaller than that of other specimens (Fig. 6). In this section, reasons for the acceleration in the grain refinement due to the pre-existing precipitates are discussed.

One of the possible reasons for the grain-refinement acceleration is an influence of the pre-existing precipitates on dislocation motion during plastic deformation. It has been reported that precipitates can increase the rate of dislocation generation by encouraging the formation of Orowan and prismatic loops, as has been reported in the references.[10,18,26–29] At the same time, precipitates inhibit the long-range migration of dislocations, so that uniform slip of dislocations become difficult and development of local deformation zones containing large local misorientation gradients is promoted. Barlow *et al.* have reported an accelerated grain refinement in precipitate bearing aluminum as well as enhanced dislocation generation and a reduction in the slip distances.[30] The relationship between dislocation density in a specimen with precipitates, ρ_D, and in a precipitate free alloy, ρ_s, can be described by following equations.[27,31]

$$\frac{\rho_D}{\rho_s} = \frac{3 f_v L}{r} \quad (1)$$

where f_v, r and L are the volume fraction of precipitates, mean radius of precipitates and slip length in the single-phase alloy, respectively. Equation (1) gives approximately an order of magnitude increase in dislocation density in the specimen

with precipitates relative to that in a precipitate free specimen.[31] The increase in dislocation density naturally leads to increase the formation rate of HAGBs. In the TEM micrographs, high-density of dislocations were actually observed in the Aged-specimens (Fig. 8). Actually, the fraction of HAGBs in the Aged-specimens was higher than that in the ST-specimen during the ARB process. Moreover, the fraction of HAGBs in the 300°C Aged-ARB specimen was higher than that of the 400°C Aged-ARB specimen. The results can be explained by the expected increase in the dislocation multiplication rate in the 300°C Aged-ARB specimen having finer precipitates than those in the 400°C Aged-ARB specimen. It is now summarized that the pre-existing precipitates increase the rate of dislocation multiplication and accumulation then accelerate the HAGBs formation during the ARB process.

As was mentioned above, large number of precipitates inhibit uniform dislocation slips and result in inhomogeneous deformation and rather instability like shear banding. Introduction of shear bands during SPD processes have been reported in previous literatures.[10,11,21–23] Introduction of shear bands also results in subdivision of original crystals, especially subdivision of elongated or lamellar grains. Thus, another possible reason for the acceleration in grain refinement might be shear banding during the ARB process. Actually, the shear bands were observed in the Aged-ARB specimens (Fig. 7), while they were hardly observed in the ST-ARB specimen. It seems from the EBSD boundary maps (Fig. 4) that the shear bands were mainly introduced at low ARB cycles. Furthermore, the number of the shear bands introduced by the ARB process in the 300°C Aged-ARB specimen was larger than that in the 400°C Aged-ARB specimen (Fig. 7), probably because finer and denser precipitates made uniform slips more difficult. It corresponds to the experimental result that the grain size of the 300°C Aged-ARB specimen was smaller than that of the 400°C Aged-ARB specimens at low ARB cycles (Fig. 6). Therefore, it is concluded here that the pre-existing precipitates inhibit uniform dislocation slips in the matrix to result in also strain localization like shear banding, which leads to acceleration of grain refinement during the ARB process, especially at low ARB cycles. In addition, the effect of finer precipitate is more effective on the acceleration.

By the way, it was found that the grain size (the thickness of grains) saturated above 7 cycles of ARB cycles from the microstructural observation [Fig. 6(a)]. The result suggests that a kind of microstructure coarsening including boundary migration occurs during the ARB process. Such a microstructure coarsening during the ARB process is probably affected by the pre-existing precipitates. Thus, the interaction between the precipitates and grain boundaries is also considered as another effect of the pre-existing precipitates on microstructural evolution during the ARB process. Figure 15 shows TEM micrographs of the 400°C Aged-ARB specimen after 9 cycles. In the figures, a wavy boundary is found to be pinned by the precipitates. This indicates that the grain boundary migration happened during the ARB process. It is well known that fine precipitate can inhibit grain boundary migration by so-called Zener drag effect. The Zener dragging force, F, is shown as follows:

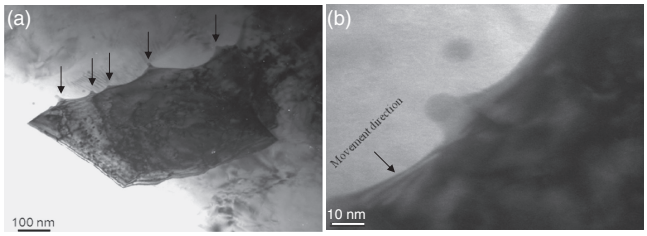

Fig. 15 TEM micrographs of the 400°C Aged-ARB specimen after 9 cycles showing interaction between Al_3Sc and the boundaries.

$$F = 3/8(f/r^2)\gamma D_{sg} \approx 1/r^2 \quad \text{for a low-angle boundary} \quad (2)$$
$$F = 3/2(f/r)\gamma \approx 1/r \quad \text{for a high-angle boundary} \quad (3)$$

where f is the volume fraction of second phase particle, r is the particle radius, D_{sg} is the subgrain size and γ is the surface energy. It is found that F becomes larger when the Al_3Sc precipitates have finer size and keep identical orientation with the matrix, which results in lower surface energy.[32,33] In the experimental results, the thicknesses of the elongated grains after 10 cycles were 0.24, 0.27 and 0.37 μm for the 300°C Aged-ARB, 400°C Aged-ARB and ST-ARB specimens, respectively. The grain size of the Aged-ARB specimens is smaller than that in the ST-ARB specimen. And the specimens with the finer pre-existing precipitates showed smaller grain sizes. The results also agree with the magnitude of Zener dragging force expected from the eqs. (2) and (3). Hence, it is also concluded that the Aged-ARB specimens having the pre-existing precipitates showed smaller grain size than the ST-ARB specimen because the pre-existing precipitates inhibited the grain boundary migration during the ARB process. However, we should note that the ultrafine grained structures in the ARB processed specimens are not controlled only by the grain growth but are the results of grain subdivision during heavy plastic deformation. Therefore, the Zener drag would give just a minor effect on microstructure evolution at high ARB cycles.

It can be concluded that the important roles of the pre-existing precipitation in the microstructural evolution during the ARB process are firstly to increase the generation and accumulation rate of dislocation and secondarily to introduce shear bands at low ARB cycles, as well as to inhibit the grain boundary migration at high ARB cycles as a minor effect. The roles of the pre-existing precipitation lead to acceleration of grain refinement and decrease in grain size during the ARB process.

5. Conclusions

Microstructural evolution during severe plastic deformation by ARB process up to 10 cycles (equivalent strain of 8.0) in a solution treated specimen and pre-aged specimens aged at 300°C or 400°C of an Al–0.2% Sc alloy was investigated. The main results are summarized as follows:

(1) Coherent precipitates of Al_3Sc with mean particle size of 50 nm which showed a cauliflower-like shape were observed after aging at 400°C for 10 ks. On the other hand, fine and spherical coherent precipitates with mean particle size of 3.6 nm were found after aging at 300°C.

(2) After 10 cycles of ARB, lamellar boundary structures were observed in all the specimens. The mean grain thickness of the elongated ultrafine grains in the Aged-ARB specimens containing precipitates was smaller than that in the ST-ARB specimen. The fraction of high angle grain boundaries (HAGBs) and the average misorientation in the Aged-ARB specimens were larger than those in the ST-ARB specimen. The results show that pre-existing Al_3Sc precipitates accelerated the grain refinement during the ARB process.

(3) The acceleration of the grain refinement is considered to be caused by the increase in the dislocation generation rate due to the pre-existing precipitates as well as by the introduction of shear bands. After many cycles of the ARB process, the saturated grain sizes in the Aged specimens were smaller than that in the ST-specimen. The precipitates also play an additional role to inhibit short range grain boundary migration at later stage of ARB through Zener drag effect. It was also found that the effects of the finer pre-existing precipitates in the 300°C Aged-ARB specimens on grain refinement were more effective than that of the coarse precipitate in the 400°C Aged-ARB specimens.

(4) From the TEM observations, it was found that the state of the precipitates changed during the ultrahigh strain deformation by ARB process. The coherency between the precipitates and Al matrix was kept during 1 cycle of ARB process. However, some precipitates have different orientation relationship with matrix after 9 cycles. Additionally, the cauliflower shaped precipitates observed in the 400°C Aged-ARB specimens were changed to the fine and spherical-shaped ones after many ARB cycles. From the results, it was expected that the Al_3Sc precipitates were dissolved and re-precipitated, or fragmented by plastic deformation during the ARB process.

Acknowledgement

This study was financially supported by the Grant-in-Aid for Scientific Research on Innovative Area, “Bulk Nano-structured Metals”, through MEXT, Japan. The support was gratefully acknowledged.

REFERENCES

1) R. Z. Valiev, R. K. Islamgaliev and I. V. Alexandrov: Prog. Mater. Sci. **45** (2000) 103–189.
2) R. Z. Valiev, Y. Estrin, Z. Horita, T. G. Langdon, M. J. Zehetbauer and Y. T. Zhu: JOM **58** (2006) 33–39.
3) R. Z. Valiev, R. K. Islamgaliev and I. V. Alexandrov: Prog. Mater. Sci. **24** (2000) 103.
4) V. Jindal, P. K. De and K. Venkateswarlu: Mat. Lett. **60** (2006) 3373–3375.
5) J. Gubicza, I. Schiller, N. Q. Chinh, J. Illy, Z. Horita and T. G. Langdon: Mater. Sci. Eng. A **460–461** (2007) 77–85.
6) E. A. Marquis and D. N. Seidman: Acta Mater. **49** (2001) 1909–1919.
7) G. M. Novotny and A. J. Ardell: Mater. Sci. Eng. A **318** (2001) 144–154.
8) B. K. Min, H. W. Kim and S. B. Kang: Mater. Process. Technol. **162–163** (2005) 355–361.
9) F. J. Humphreys and P. B. Hirsch: Philos. Mag. **34** (1976) 373.
10) F. J. Humphrey: Acta Metall. **27** (1979) 1801.
11) H. Jazeri and F. J. Humphreys: D. A. Gottstein, D. A. Molodov (ed.), 5th Int. Conference on Recrystallization and Related Annealing Phenomena. Belgium, (2001) p. 549.
12) P. J. Apps, J. R. Bowen and P. B. Prangnell: M. Zehetbauer, R. Z. Valiev (Ed.), Nanomaterials by Severe Plastic Deformation-NANSPD2, Vienna Austria, December, (2002) p. 138.
13) P. J. Apps, J. R. Bowen and P. B. Prangnell: Acta Mater. **51** (2003) 2811.
14) F. J. Humphreys: *Dislocations and Properties of Real Materials*, ed. by M. H. Loretto, London (1984) p. 175.
15) P. J. Apps, M. Berta and P. B. Prangnell: Acta Mater. **53** (2005) 499–511.
16) H. Jazaeri and F. J. Humphreys: Acta Mater. **52** (2004) 3251.
17) M. Z. Quadir, M. Ferry, O. Al-Buhamad and P. R. Munroe: Acta Mater. **57** (2009) 29–40.
18) S. H. Lee, Y. Saito, T. Sakai and H. Utsunomiya: Mater. Sci. Eng. A **325** (2002) 228–235.
19) H. Pirgazi, A. Akbarzadeh, R. Petrov and L. Kestens: Mater. Sci. Eng. A **497** (2008) 132–138.
20) S. Li, F. Sun and H. Li: Acta Mater. **58** (2010) 1317–1331.
21) A. Goloborodko, O. Sitdikov, T. Sakai, R. Kaibyshev and H. Miura: Mater. Trans. **44** (2003) 766.
22) O. Sitdikov, T. Sakai, E. Avtokratova, R. Kaibyshev, Y. Kimura and K. Tsuzaki: Mater. Sci. Eng. A **18** (2007) 444.
23) O. Sitdikov, T. Sakai, A. Goloborodko, H. Miura and R. Kaibyshev: Philos. Mag. **85** (2005) 1159.
24) N. Tsuji, Y. Saito, S. H. Lee and Y. Minamino: Adv. Eng. Mater. **5** (2003) 5.
25) R. Song, D. Ponge, D. Raabe, J. G. Speer and D. K. Matlock: Mater. Sci. Eng. A **441** (2006) 1.
26) F. J. Humphreys and M. G. Ardakani: Acta Metall. Mater. **42** (1994) 749.
27) P. B. Hirsch and F. J. Humphreys: *Physics of Strength and Plasticity*, ed. by A. S. Argon, (MIT Press, 1969) p. 189.
28) P. J. Apps, M. Berta and P. B. Prangnell: Acta Mater. **53** (2005) 499.
29) M. F. Ashby: Philos. Mag. **21** (1970) 399.
30) C. Y. Barlow, N. Hansen and Y. L. Liu: Acta Mater. **50** (2002) 171.
31) D. Hull and D. J. Bacon: *Introduction to Dislocations*, 3rd ed., (Oxford: Pergamon Press, 1984) p. 69.
32) L. S. Toropova, D. G. Eskin, M. L. Kharakterova and T. V. Dobatkina: *Advanced Aluminum Alloys Containing Scandium*, (Gordon and Breach Science, 1998).
33) F. J. Humphreys and M. Hatherly: *Recrystallization and Related Annealing Phenomena*, (Pergamon Press, 1995).